Optimal Planning of Distributed Generators and Shunt Capacitors in Isolated Microgrids with Nonlinear Loads

Ameen H. Yazdavar, *Student Member, IEEE*, Mostafa F. Shaaban, *Member, IEEE*, Ehab F. El-Saadany *Fellow, IEEE* and M. M. A. Salama *Fellow, IEEE*

Abstract—This paper presents a comprehensive design procedure for isolated microgrids with a high penetration of nonlinear loads. The proposed microgrid planning approach simultaneously determines the sizes, locations and types of distributed generators (DGs) and shunt capacitor banks (CBs). The presence of nonlinear loads along with the capacitors of CBs or DGs' output filters may cause severe voltage distortions. To consider this issue, a harmonic power flow tool suitable for planning is developed that takes into account the specific features of isolated microgrids. Moreover, to consider the necessity of supply continuity for isolated microgrids after a contingency, a reliability-based method is proposed that allows building successful islands. Unlike previous methods, the one proposed here does not rely merely on supply adequacy, and takes into account the fact that the voltage provision requirement can only be fulfilled through the dispatchable DGs. The intermittent natures of loads and renewable DGs are modelled probabilistically. The effectiveness of the proposed planning approach has been validated using the PG&E 69-bus system.

Index Terms—isolated microgrids, distributed generators, capacitor banks, harmonic power flow, nonlinear loads, reliability

NOMENCLATURE

A. Indices

b	Index for bus.
s_g, s_l, s_c	Indices for generation, load, and configuration states.
s	Index for combined states of wind-power generation and load.
s^M	Index for state corresponding to maximum wind-power generation and load.
bk	Index for feeder between buses b and k.
y, day, hr	Indices for year, day, and hour.
t	Index for time $[y, day, hr]$.
db, wb, cb	Indices for candidate buses of diesel generators, wind turbines and capacitor banks.
dr, wr, cr	Indices for available ratings of diesel generators, wind turbines and capacitor banks.

B. Sets

$\mathcal{S}^B$	Set of all buses.
$\mathcal{S}^C$	Set of all system configurations.
$\mathcal{S}^S$	Set of system states.
$\mathcal{S}^{DB}, \mathcal{S}^{WB}, \mathcal{S}^{CB}$	Sets of candidate buses for diesel generators, wind turbines, and capacitor banks.
$\mathcal{S}^{DR}, \mathcal{S}^{WR}, \mathcal{S}^{CR}$	Sets of available ratings for diesel generators, wind turbines, and capacitor banks.
$\mathcal{S}^G, \mathcal{S}^L, \mathcal{S}^C$	Sets of system generation, load, and configuration states.

C. Costs and Constants

$C_{dr}^C, C_{wr}^C, C_{cr}^C$	Capital costs of diesel generators, wind turbines, and capacitor banks.
M_{dr}^C, M_{wr}^C	Maintenance costs of diesel generators and wind turbines.
F^C	Fuel cost.
H^R	Heat rate.
K^P	Allowed penetration for renewable DGs.

D. Parameters

$P_{dr}^{max}, P_{dr}^{min}$	Max. and min. active power limits of diesel generator dr.
Q_{dr}^{max}	Min. reactive power limit of diesel generator dr.
m_{dr}^P	$\omega - P$ droop gain of diesel generator dr.
m_{dr}^Q	$V - Q$ droop gain of diesel generator dr.
S_{dr}, S_{cb}	Ratings of diesel generator dr and capacitor bank cb.
$\Delta\omega^{per}$	Permissible frequency drop.
ΔV^{per}	Permissible voltage drop.
ω^{nom}, V^{nom}	Nominal frequency and voltage.
V^{max}, V^{min}	Permissible bus max. and min. voltages.
D^R	Discount rate.
$LOLE^U$	Upper limit for $LOLE$.
N^B	Number of buses.
$\Pr_s$	Probability of state s.
$THD^{V,U}, IH^{V,U}$	Upper limits for voltage THD and IH.

E. Variables

$P_{wr,t,s}$	Power injected by wind turbine wr, at time t for state s.
$P_{dr,t,s}, Q_{dr,t,s}$	Active and reactive powers of diesel generator dr, at time t for state s.
$P_{b,t,s}^I, Q_{b,t,s}^I$	Active and reactive powers injected by network into bus b, at time t for state s.
$P_{b,t,s}^L, Q_{b,t,s}^L$	Active and reactive powers of bus b load, at time t for state s.
$LOLE$	Loss of load expectation.
V, δ	Bus voltage magnitude and phase angle.
Y_{bk}, θ_{bk}	Admittance magnitude and angle between buses b and k.
$x_{db,dr}$	Binary variable for installing diesel generator dr at candidate bus db.
$x_{wb,wr}$	Binary variable for installing wind turbine wr at candidate bus wb.
$x_{cb,cr}$	Binary variable for installing capacitor bank cr at candidate bus cb.
$y_{cb,cr,s}$	Binary variable for operation of capacitor bank cr at candidate bus cb for state s.
$THD_{b,t,s}^V, IH_{b,t,s}^V$	THD^V and IH^V of bus b, at time t for state s.
V	Bus voltage phase angle.

I. INTRODUCTION

MICROGRIDS, as clusters of loads and distributed generators (DGs), have already been acknowledged by IEEE Std. 1547.4 to maintain the service of critical loads when a supply grid is not available [1]. Continuation of service in such islanded modes can provide significant cost saving. On the other hand, high energy costs and environmental aspects have motivated energy participants to integrate renewable generators into microgrids so that they are rarely seen without renewable generators. Along with grid-connected microgrids, in off-grid regions such as remote communities [2], mines [3], islands [4] and military centers [5], isolated microgrids can be found, in which the issues relevant to fuel transportation are also added to the above motivations for using renewable generators.

Optimal DG placement, in general, is necessary to achieve a microgrid's potential benefits with respect to its high investment cost. Although islanded and isolated microgrids have almost equivalent operational and control requirements, they are different from a planning point of view, mainly due to the short time of microgrid operation in the islanded mode [6]. Accordingly, in the case of grid-connected microgrids, the islanded mode requirements hardly

ever become dominant planning constraints. However, an isolated microgrid needs its special features to be considered within the planning. These features include the necessity of providing voltage and frequency support for the microgrid by some of the DGs, essentially by diesel generators [7]. To satisfy the reliability constraints, these voltage-controlled DGs should be distributed throughout the islolated microgrids, which has not been included so far in the planning. Further, in isolated microgrids, some DGs are operated based on droop characteristics. Unlike grid-connected microgrids, in which the frequency and voltage are dictated by the main grid, application of droop characteristics, frequency-active power and voltage-reactive power, for isolated microgrids causes the frequency and voltage to deviate from their nominal values [8]. As will be explained, the droop characteristics, especially the voltage-reactive power one, affect the sizes of DGs and should be merged into the planning formulation, which has not been done yet. Moreover, if a high penetration of nonlinear loads exists, harmonic analysis suitable for planning of isolated microgrid should be carried out to ensure the power quality constraints in terms of voltage distortions are met.

On the other hand, capacitor banks (CBs) have always been regarded as the most economic solution for volt/var control and power loss reduction of distribution systems [9]. Considering the reality of modern distribution systems, DGs and CBs coexist, and they share some of their operational tasks. Thus, to maximize the benefits, DGs and CBs must be simultaneously sited and sized. This point has been propounded in [10] for active distribution networks (ADNs); however, a different formulation is required for an isolated microgrid to incorporate its specific features, which has not been addressed in the literature. Additionally, capacitors affect the flow of harmonic currents and may cause resonance and high voltage distortion levels [9]. This fact emphasizes the need for harmonic power flow considerations in the planning of microgrids penetrated with nonlinear loads.

Optimal planning of isolated microgrids has been tackled in a number of studies. The research in [2] carried out the planning for sizing different types of DGs. In [11], a coordinated sizing of energy storage and diesel generators have been proposed by applying the discrete Fourier transform. The authors in [12] proposed a long-term planning to size renewable DGs for Canadian remote communities to maximize the communities' social welfare. This work has been ameliorated in [13] by adding energy storage units. However, these works included neither the features relevant to the droop-based operation of isolated microgrids, nor the distribution of voltage controlled DGs in the planning. Moreover, DGs have been considered as the main source of reactive power, and the need for CBs and corresponding harmonic analysis have been ignored.

By contast, incorporating a harmonic power flow in the planning of ADNs has already been suggested. A probabilistic optimal planning for renewable DGs was propounded in [14] to minimize the annual power loss of a typical rural distribution feeder with a high penetration of nonlinear loads. Since this research was performed on an ADN, the specific features of isolated microgrids have not been considered in the planning. The planning objective in [15] is to determine the optimal location and size of current-controlled DGs for a distribution network, considering harmonic and protection limits. The only source of non-linearity investigated in this work are the DGs that are modeled by the emission limits of international standards. It is shown that planning solution is affected by considering voltage harmonic constraint. However, the proposed method is not applicable for isolated microgrids, because of the presence of droop-based voltage controlled DG and other non-linearity resources, e.g., variable speed drives or unified power flow chargers of electric vehicles. Moreover, the above works suffer from the application of over-simplified models for inverter-based DGs, such as type III wind turbines, given that these DGs can lead to resonance due to the possibility of mutual interaction between a DG's output filter and control system on the one hand, and the distribution

system on the other hand [16], [17].

In response to the aforementioned shortcomings, this paper proposes a planning platform for isolated microgrids with nonlinear loads to simultaneously allocate DGs and CBs, considering the specific features of isolated microgrids. The main contributions of this paper are as follows:

- Simultaneously allocating DGs and CBs while considering the power quality constraints.
- Considering the specific features of isolated microgrids in fundamental and harmonic power flow algorithms, including lack of slack bus, and the droop-based nature of some DGs.
- Modelling of wind turbines in the harmonic power flow to take into account the possibility of resonance that might happen in the presence of wind turbines.
- Developing a reliability-based technique to build successful islands with dynamic borders, as a consequence of contingency.

II. PROBLEM FORMULATION

In this section, the mathematical model of the proposed planning problem for allocation of DGs and CBs is described. The problem is formulated as a mixed-integer non-linear programming (MINLP). The following assumptions are made: 1) The problem is an extensional planning one in which the available microgrid network is initially supplied by diesel-generator units connected to the generating bus. Due to ageing, the diesel generators are to be replaced by new units. 2) DGs' and CBs' capacities are discretized at definite steps. 3) All DGs belong to the same entity. 4) The renewable DGs are assumed to operate at unity power factor to harvest their maximum available power.

A. Objective Function

The planning objective is to minimize the total expected planning cost, once levelized over the planning horizon, considering the probability of each load-generation state. The derivation of load-generation model is explained in Section V. Considering the decision variable $\mathcal{X}$ as the sizes, locations, and types of DGs and CBs, the objective function is described by

$$\min_{\mathcal{X}} \sum_{s \in \mathcal{S}^S} \Pr_s \left(C^C + O_s^C + M^C \right) \tag{1}$$

where C^C, O_s^C, M^C are the levelized capital, operational and maintenance costs.

Levelizing the costs are performed using two factors: capital recovery factor (CRF) and levelizing factor (LF) [18]. CRF is used to annualize the capital cost, and LF is applied to convert the escalating annual operational and maintenance costs into a series of equal amounts. These factors are given by

$$CRF = \frac{i(1+i)^n}{(1+i)^n - 1} \tag{2}$$

$$LF = \frac{(1+d')^n - 1}{d'(1+d')^n} \frac{d(1+d)^n}{(1+d)^n - 1} \tag{3}$$

where i and d are the interest and discount rates, respectively; and $d' = (d-e)/(1+e)$, where e is the escalation factor.

The cost terms in (1) can be written as

$$
\begin{aligned}
C^C =& CRF \left(\sum_{db \in \mathcal{S}^{DB}} \sum_{dr \in \mathcal{S}^{DR}} x_{db,dr} C_{dr}^C + \right. \\
& \left. \sum_{wb \in \mathcal{S}^{WB}} \sum_{wr \in \mathcal{S}^{WR}} x_{wb,wr} C_{wr}^C + \sum_{cb \in \mathcal{S}^{CB}} \sum_{cr \in \mathcal{S}^{CR}} x_{cb,cr} C_{cr}^C \right)
\end{aligned}
\tag{4}
$$

$$O_s^C = LF \left(\sum_{day=1}^{365} \sum_{hr=1}^{24} \sum_{db \in \mathcal{S}^{DB}} \sum_{dr \in \mathcal{S}^{DR}} x_{db,dr} P_{d,t,s} H^R F^C \right) \quad (5)$$

$$M^C = LF \left(\sum_{db \in \mathcal{S}^{DB}} \sum_{dr \in \mathcal{S}^{DR}} x_{db,dr} M_{dr}^C \right.$$
$$\left. + \sum_{wb \in \mathcal{S}^{WB}} \sum_{wr \in \mathcal{S}^{WR}} x_{wb,wr} M_{wr}^C \right) \quad (6)$$

B. Constraints

1) Power Flow Equations: Equations (7) and (8) describe the balancing constraints of active and reactive powers, respectively. In these equations, the terms describing the injected powers are defined by (9)–(14): the active and reactive powers of the lines (9, 10), the active power of wind turbines (11), the reactive power of capacitor banks (12), and the active and reactive powers of diesel generators (13, 14). Additionally, the power flow equations of isolated microgrids should account for the lack of a slack bus, and the droop-based operation of some DGs. The study conducted in [19] has shown that these characteristics impact: 1) the microgrid frequency, and consequently, bus voltages' angles and the flow of power and 2) the bus voltages' magnitudes. Further, obtaining accurate results entails the application of a different power flow algorithm than the conventional one.

It is emphasized here that the above-mentioned characteristics must be embedded in the planning of isolated microgrids for the following reasons: 1) to investigate more accurately the planning constraints, and more importantly, 2) to account for the impact of voltage-reactive power droop characteristic. Although the droop characteristics, frequency-active power and voltage-reactive power, are employed to evenly distribute loads' active and reactive powers among generators, the error of reactive power sharing can be significant [20]. This error is a function of DGs' locations and their feeder impedances [21], and thus, must be considered in the planning. To account for the effect of droop characteristics, (15) and (16) are applied, whose droop slopes are given by (17) and (18), respectively, and are defined in terms of generator ratings and the permissible frequency and voltage drops. Further, another constraint on the reactive power of droop-based DGs will be added in the next subsection.

$$P_{b,t,s}^I + P_{b,t,s}^W + P_{b,t,s}^D - P_{b,t,s}^L = 0, \forall b, t, s \quad (7)$$

$$Q_{b,t,s}^I + Q_{b,t,s}^C + Q_{b,t,s}^D - Q_{b,t,s}^L = 0, \forall b, t, s \quad (8)$$

$$P_{b,t,s}^I = \sum_{k=1}^{N^B} V_{b,t,s} V_{k,t,s} Y_{bk,s} \cos (\delta_{b,t,s} - \delta_{k,t,s} - \theta_{bk,t,s}) \quad (9)$$

$$Q_{b,t,s}^I = \sum_{k=1}^{N^B} V_{b,t,s} V_{k,t,s} Y_{bk,s} \sin (\delta_{b,t,s} - \delta_{k,t,s} - \theta_{bk,t,s}) \quad (10)$$

$$P_{b,t,s}^W = \sum_{wr \in \mathcal{S}^{WR}} x_{b,wr} P_{wr,t,s} \quad (11)$$

$$Q_{b,t,s}^C = \sum_{cr \in \mathcal{S}^{CR}} x_{b,cr} y_{b,cr,s} Q_{cr,t,s} \quad (12)$$

$$P_{b,t,s}^D = \sum_{dr \in \mathcal{S}^{DR}} x_{b,dr} P_{dr,t,s} \quad (13)$$

$$Q_{b,t,s}^D = \sum_{dr \in \mathcal{S}^{DR}} x_{b,dr} Q_{dr,t,s} \quad (14)$$

$$P_{dr,t,s} = \frac{1}{m_{dr}^P} (\omega^{nom} - \omega_{t,s}) \quad (15)$$

$$Q_{dr,t,s} = \frac{1}{m_{dr}^Q} (V^{nom} - V_{t,b,s}) \quad (16)$$

$$m_{dr}^P = \frac{S_{dr}}{\Delta \omega^{per}} \quad (17)$$

$$m_{dr}^Q = \frac{S_{dr}}{\Delta V^{per}} \quad (18)$$

where $b \in \mathcal{S}^B$ and $s \in \mathcal{S}^S$.

2) Network's Elements: An additional set of constraints is related to the network's elements, including the capacity of DGs, CBs, and feeders along with the penetration level of renewable DGs and bus voltage limits, as given by (19)–(25). Specifically, (21) recommends

considering zero as the minimum reactive power limit of diesel generators, i.e., only over-excited behaviour is allowed for isolated microgrids, for the following reason. According to the voltage-reactive power droop characteristic, as given by (16), if the voltage of a diesel unit goes above the nominal voltage, the reactive power of that generator becomes negative, and the generator is operated in an under-excited mode. In this case, the generator's reactive power demand is supplied by the rest of generators, and accordingly, the rating of the other generators must be increased. To avoid such scenarios, the under-excited behaviour of diesel generators is excluded.

$$\sqrt{P_{dr,t,s}^2 + Q_{dr,t,s}^2} \leq x_{b,dr} S_{dr}, \forall b, dr, t, s \quad (19)$$

$$x_{b,dr} P_{dr}^{\min} \leq P_{dr,t,s} \leq x_{b,dr} P_{dr}^{\max}, \forall b, dr, t, s \quad (20)$$

$$0 \leq Q_{dr,t,s} \leq x_{b,dr} Q_{dr}^{\max}, \forall b, dr, t, s \quad (21)$$

$$Q_{cb,t,s} \leq x_{b,cr} S_{cr}, \forall b, cr, t, s \quad (22)$$

$$I_{bk,t,s} \leq I_{bk}^{\max}, \forall bk, t, s \quad (23)$$

$$V^{\min} \leq V_{t,b,s} \leq V^{\max}, \forall b, t, s \quad (24)$$

$$\sum_b P_{b,s^M}^W \leq K^P \sum_b P_{b,s^M}^D \quad (25)$$

where $b \in \mathcal{S}^B$, $dr \in \mathcal{S}^{DR}$, $s \in \mathcal{S}^S$.

It is worth noting that the above-mentioned negative reactive power, which might be supplied by some of the generators, has the same reason as that of reactive-power-sharing-error, referred to in the previous subsection. They are due to the difference in generators' feeder impedances. Because the generators' terminal voltage in (10) is not a global parameter and differs for different generators, the network-demanded reactive power is not shared accurately among generators, and in specific situations, some generators might supply negative reactive powers. Given that an isolated microgrid is operated based on droop characteristics, the operational consequences of their application must be considered in the planning, which as explained, requires a suitable model for power flow, and an additional constraint prohibiting under-excited behaviour of diesel generators.

Algorithm 1 The LOLE Calculation

1: Start $\Pr_{fail} = 0$
2: **for all** $s_c \in \mathcal{S}^C$ **do**
3:     Read $island_1$ and $island_2$
4:     **for all** $s_g \in \mathcal{S}^G$ **do**
5:         **for all** $s_l \in \mathcal{S}^L$ **do**
6:             Calculate $\Pr_{c,g,l} = \Pr_c \Pr_g \Pr_l$
7:             **for all** $island \in \{island_1, island_2\}$ **do**
8:                 **if** $island$ is not successful **then**
9:                     Calculate $\Pr_{fail} = \Pr_{fail} + \Pr_{c,g,l}$
10:                 **end if**
11:             **end for**
12:         **end for**
13:     **end for**
14: **end for**
15: Calculate $LOLE = 8760 \Pr_{fail}$

---

3) Reliability: The North American Electric Reliability Corporation (NERC) standards mandate power systems to meet the $N-1$ security constraint, i.e., the system must continue its normal operation after any single element failure [22]. After a fault occurrence on any distribution line of an isolated microgrid and the fault removal, two separate islands are built. Depending on the fault location, the size of the islands can be significant, in which case under the NERC recommendations, neither can be ignored and both must operate normally. Compared to ADNs, building successful islands in the case of isolated microgrids is more important, given that isolated

microgrids are located in the off-grid regions with minimal access to other facilities.

On the other hand, the renewable DGs such as wind turbines and photovoltaic panels are categorized under the grid-feeding DGs, meaning that they cannot provide voltage and frequency support for the system [23]. These renewable DGs are connected to power systems through voltage-source-converters operated under the current-controlled mode to harvest their maximum available power, and accordingly, they are furnished with neither voltage control capability nor droop characteristics [24]. Therefore, although satisfying the supply adequacy constraint, an island comprising only renewable DGs such as wind turbines is doomed to failure. To avoid this failure, voltage controlled DGs should be distributed throughout an isolated microgrid to satisfy the reliability constraint developed in this subsection.

The reliability constraint is evaluated here based on $LOLE$ derived for a composite generation-load-network model that takes into account the stochastic behaviour of the wind turbines and loads as well as the failure possibility of diesel generators, wind turbines, and distribution lines. First, all possible configurations caused by any distribution line fault removal are generated. Each configuration comprises two islands. An island is considered successful if, in addition to meeting its active and reactive power demands, it has a voltage-control DG, which here is a diesel generator. Then, for all states of the generation and load as well as all configurations caused by the fault removals, $LOLE$ is calculated considering the states' corresponding probabilities as described by Algorithm 1. The obtained $LOLE$ should be less than its predefined upper limit, $LOLE^U$ as

$$LOLE \leq LOLE^U \tag{26}$$

4) Voltage Distortion: The proliferation of nonlinear loads in distribution systems results in voltage-harmonic-distortion, one of the most significant power quality problems. Moreover, shunt capacitors are distributed throughout the distribution system as the source of reactive power or in the DGs' output filters. The presence of capacitors may lead to quasi-resonance [17], in which a harmonic frequency is near to the resonant frequency of the impedance network, and accordingly, aggregates the voltage distortion. Since the voltage distortion is affected by the size and location of DGs and CBs, harmonic analysis and voltage-distortion constraints should be embedded in the planning. As the harmonic analysis, in this paper, a harmonic power flow algorithm suitable for the planning of isolated microgrids is developed, and is elaborated on in Section III. As the voltage-distortion constraints, the upper limits of voltage total-harmonic-distortion (THD^V) and individual-harmonic-distortion (IH^V) are considered, as offered by the international standards in [25] and [26]. These constraints are checked at all microgrid buses and formulated as

$$THD^V_{b,t,s} \leq THD^{V,U}, \forall b, t, s \tag{27}$$

$$IH^V_{b,t,s} \leq IH^{V,U}, \forall b, t, s \tag{28}$$

where $b \in \mathcal{S}^B$ and $s \in \mathcal{S}^S$.

5) Binary Variables: The following constraints are considered for binary variables. Specifically, (30)-(32) are included to ensure only one member of each set can be installed at each candidate bus.

$$x_{db,dr},\ x_{wb,wr},\ x_{cb,cr},\ y_{cb,cr,s} \in \{0,1\} \tag{29}$$

$$\sum_{dr \in \mathcal{S}^{DR}} x_{db,dr} \leq 1, \quad \forall db \in \mathcal{S}^{DB} \tag{30}$$

$$\sum_{wr \in \mathcal{S}^{WR}} x_{wb,wr} \leq 1, \quad \forall wb \in \mathcal{S}^{WB} \tag{31}$$

$$\sum_{cr \in \mathcal{S}^{CR}} x_{cb,cr} \leq 1, \quad \forall cb \in \mathcal{S}^{CB} \tag{32}$$
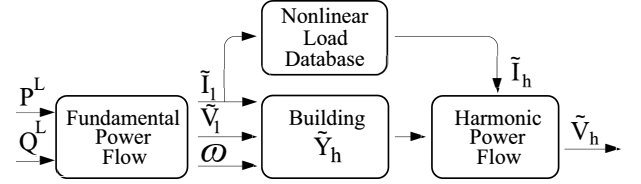

Fig. 1. Harmonic power flow for isolated microgrids.

III. HARMONIC POWER FLOW

In this section, a harmonic power flow algorithm suitable for planning studies of isolated microgrids is proposed. The proposed algorithm is shown in Fig. 1. As can be seen, the fundamental power flow introduced in the Section II provides the inputs for harmonic analysis, and accordingly, takes into account the fact that isolated microgrids are formed based on droop-based DGs and there is no slack bus. The fundamental power flow takes the vectors of load active and reactive powers, $\mathbf{P^L}$ and $\mathbf{Q^L}$, respectively, as the inputs, and generates the vectors of fundamental voltage and current phasors, i.e., $\tilde{\mathbf{V}}_1$ and $\tilde{\mathbf{I}}_1$, respectively, as well as the system frequency ω. The harmonic analysis includes the following:

1) The nonlinear loads' harmonic spectrum are updated based on their fundamental current magnitudes and phase angles. Representing the magnitude and phase angle of the hth harmonic order obtained from the nonlinear loads' database by $I_{h,spec}$ and $\theta_{h,spec}$, respectively, one can write [27]:

$$\theta_h = \theta_{h,spec} + h\left(\theta_1 - \theta_{1,spec}\right) \tag{33}$$

$$I_h = I_1 \frac{I_{h,spec}}{I_{1,spec}} \tag{34}$$

where I_1 and θ_1 are the magnitude and phase angle of the fundamental current phasor, $\tilde{I}_1$. The vector of harmonic current phasor, $\tilde{\mathbf{I}}_\mathbf{h}$, is constructed using the updated spectrum of nonlinear loads.

2) The harmonic bus admittance matrix at different harmonic orders, $\tilde{\mathbf{Y}}_\mathbf{h}$ is generated using:
   - The dispatchable DGs' and distribution lines' admittances.
   - The CB's shunt admittances, as

$$\tilde{Y}_{b,h} = jh\omega S_{cb,b} \tag{35}$$

   - An equivalent harmonic admittance of each linear loads, as given by (36) and (37).

$$\tilde{Y}_{b,1} = \frac{P^L_b - jQ^L_b}{V^2_{b,1}} \tag{36}$$

$$\tilde{Y}_{b,h} = \left(\text{Re}(\tilde{Y}^{-1}_{b,1}) + jh\omega \times \text{Im}(\tilde{Y}^{-1}_{b,1})\right)^{-1} \tag{37}$$

   where Re and Im operators return the real and imaginary parts, respectively; and $V_{b,1}$ is the voltage magnitude of bus b obtained from the fundamental power flow.
   - The Norton harmonic admittance of renewable DGs at each harmonic frequency, whose derivation is explained in Section IV.

3) The microgrid bus harmonic voltages are acquired by

$$\tilde{\mathbf{V}}_\mathbf{h} = \tilde{\mathbf{Y}}^{-1}_\mathbf{h} \tilde{\mathbf{I}}_\mathbf{h} \tag{38}$$

IV. RENEWABLE DGS IN HARMONIC POWER FLOW

In this section, the derivation procedure for renewable DGs' output admittances at harmonic frequencies is explained, which is based on the works performed in [28], [17], and [29]. Generally speaking, the switching frequencies of renewable DGs' voltage source converters (VSC) are high, so that these DGs do not generate low order harmonics [30]. This assumption is the basis of the harmonic analysis applied for planning in [14] and [15]; however, as shown in [28] and
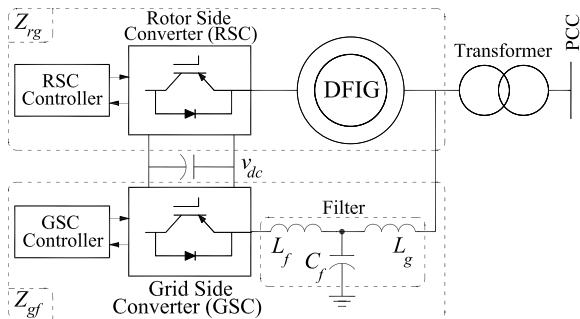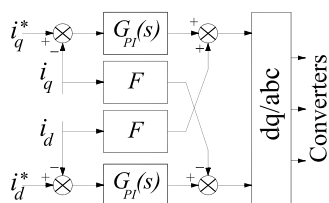
Fig. 2. DFIG configuration diagram.

Fig. 3. DFIG inner current loops.

Fig. 4. DFIG's impedance equivalent.

Fig. 5. DFIG Output Impedance.

[17], the mutual interaction among the DGs' output filters, DGs' control systems and the distribution system might lead to resonance or quasi-resonance. Therefore, the harmonic model of such DGs must be embedded in the harmonic analysis. To do so, the Norton admittance of renewable DGs, considering their control systems and output filters, are obtained and added to the harmonic bus admittance matrix. In this paper, the Norton admittance of type III wind turbines, i.e., doubly fed induction generators (DFIGs) are acquired. A similar procedure can be applied to include the harmonic models of other renewable DGs in the planning harmonic analysis.

The configuration diagram of a DFIG is shown in Fig. 2. The DFIG's wound rotor is fed by the rotor-side converter (RSC) that is controlled to deliver the required active and reactive powers from the DFIG's stator. The grid-side converter is responsible to keep the dc-link voltage, v_{dc}, at its rated value. The LCL filter at the output of GSC is applied to suppress the switching frequency harmonics. The transformer is dedicated to providing the required voltage level and preventing the flow of inrush currents once the DFIG is connected to the grid. These elements are included in the DFIG's impedance, which according to Fig. 2, consists of two parallel paths. The first path, Z_{rg}, comprises stator, rotor and the rotor-side converter. The second path, Z_{gf}, includes the filter and the grid-side converter.

The converters' impedances are affected by their controllers. Both DFIG's converters are controlled through the cascaded loops. The inner loops of both converters consist of current controllers, and their outer loops include power and voltage ones for RSC and GSC, respectively. Because the bandwidths of the power and voltage loops are far below the harmonics of interest, these loops can be neglected in the impedance model of the converters. The converters' inner-current loops are shown in Fig. 3. As can be seen, they are implemented in the dq domain [31], using proportional-integral (PI) controllers along with feed-forward controllers. The following should be considered for RSC's and GSC's impedances:

- They are obtained in the space-phasor domain [32], and accordingly, the DFIG model is also derived in the same domain.
- They are acquired using the Norton equivalent. The Norton equivalents of GSC and RSC current loops are initially obtained in the dq domain, and once shifted by $j\omega$, are transferred to the space-phasor domain.
- They are similar, and given by (39) in the space-phasor domain.

$$Z_{GSC} = Z_{RSC} = G_{PI}(s - j\omega) - jF \qquad (39)$$

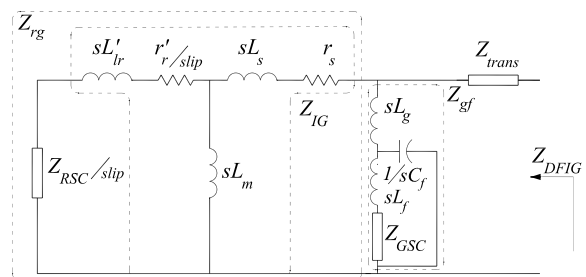where G_{PI} is the transfer function of the PI controller, and F
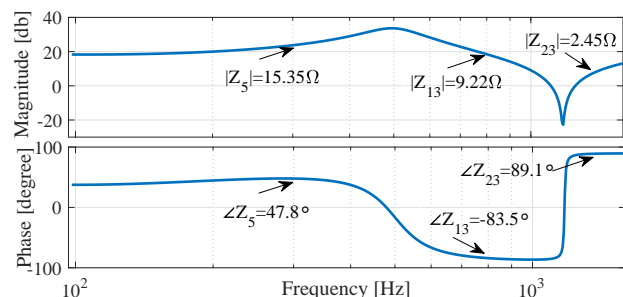
is the feed-forward gain.

- The GSC's impedance is equal in the space phasor and Laplace domains; however, RSC's impedance in the Laplace domain is obtained by dividing the one in the space phasor domain by the rotor slip in the Laplace domain, which is defined by (40).

$$slip = \frac{s - j\omega_r}{s} \qquad (40)$$

where ω_r is the rotor speed.

Having the converters' impedances, and noting the already-described impedance paths, one can construct the DFIG's impedance equivalent as show in Fig. 4, and use it to obtain the DFIG's impedance in the Laplace domain, $Z_{DFIG}(s)$. Then, the harmonic admittance of a bus with a DFIG can be written as

$$\tilde{Y}_{b,h} = \frac{1}{Z_{DFIG}(jh\omega)} \qquad (41)$$

Obtaining the DFIG's impedance, it is instructive to look at a DFIG behavior at harmonic frequencies. Fig. 5 shows the bode diagram of the output impedance of a 7.5 kW DFIG, which its parameters are given in [33]. As can be seen, at different harmonics orders, the DFIG shows different behaviours including inductive and capacitive ones. For example, at the 23th harmonic order, the phase angle is almost $90°$, and accordingly, the DFIG shows an inductive behaviour. However, at the 13th harmonic order, the phase angle is close to $-90°$, which represents a capacitor. It is worth noting that the magnitude of the DFIG's harmonic impedance are not large values, and thus, a DFIG can introduce a parallel inductive or capacitive branch to the network that must be necessarily considered in the harmonic analysis.

V. Uncertainty Modelling

This section describes the procedure for modelling the uncertainties associated with wind-power generation and load. The procedure is based on using historical data, and finding a suitable probability density function (PDF) for each source of uncertainty. Each PDF is then discretized by dividing its random variable (the uncertainty) into a number of segments, considering the trade-off between the accuracy and complexity of the planning problem. For each segment

TABLE I
LOAD STOCHASTIC MODEL

	Probability of Load States			
Load States	Winter	Spring	Summer	Fall
0.3388	0.2075	0.4887	0.2751	0.4754
0.6694	0.5574	0.4633	0.5469	0.4733
1.0000	0.2138	0.0219	0.1538	0.0255

TABLE II
WIND STOCHASTIC MODEL

	Probability of Wind States			
Wind States	Winter	Spring	Summer	Fall
0.0000	0.2503	0.1888	0.1561	0.2277
0.6500	0.3547	0.3878	0.5093	0.4073
1.0000	0.3950	0.4234	0.3346	0.3650

Fig. 6. Chromosome structure.

of a random variable, one state is assigned, whose value is given by the midpoint of that segment, and its probability is obtained using:

$$\Pr\left(x_a \le x \le x_b\right) = \int_{x_a}^{x_b} f_X\left(x\right) \tag{42}$$

where X is the random variable, x_a and x_b are the segment's bounds, and $f_X(x)$ is the PDF. Eventually, the combined wind-power generation and load model, which includes all possible operating conditions, is constructed by convolving different wind generation and load states. Denoting wind-power generation and load states by s_w and s_l, respectively, a combined wind-power generation and load state can be considered as $s = (s_w, s_l)$, whose probability is equal to $\Pr_s = \Pr_{s_w} \times \Pr_{s_l}$.

In this study, five successive years of wind-speed data have been collected. Several PDFs including Weibull, Normal and Gamma were evaluated. Using a goodness-of-fit test [34], Weibull PDF has been selected to model the wind-speed uncertainty. The data were then categorized seasonally, and four PDFs, each representing a season, were obtained. On the other hand, the output power of a wind turbine is a function of the wind speed [7]. Combining the wind power function and the PDFs of wind speed, one can determine the states of wind-power generation.

The historical data can also be used to accurately determine the load PDF. In this paper, the load is assumed to follow the pattern of IEEE reliability test system (RTS) [35], which is a common practice in the literature. The RTS provides hourly loads as the percentage of the daily peak-load for the four seasons where each season is represented by two days, a weekday and a weekend. The weekly peak-load is also described in terms of annual peak load, and accordingly, the yearly required data can be constructed. By following the same procedure as used for the wind-speed data, Normal PDF has been selected to model the load uncertainty.

Following the explained procedure, in this paper, each of wind and load stochastic models are constructed in three states for each season, as illustrated in Tables I and II, respectively.

VI. SOLUTION PROCEDURE

In the next two sub-sections, the solution procedure for already formulated optimization problem is elaborated as the main problem and a sub-problem.

A. Optimization Main Problem

The MINLP problem described in Section II is solved using genetic algorithm (GA). The chromosome structure considered for GA is illustrated in Fig. 6. As can be seen, the chromosome comprises four vectors. The first three vectors are assigned to the sizes and locations of diesel generators (DIGs), wind turbines (WTs) and capacitor banks (CBs), i.e., one vector for each type, where each vector's length is equal to the number of candidate buses. A
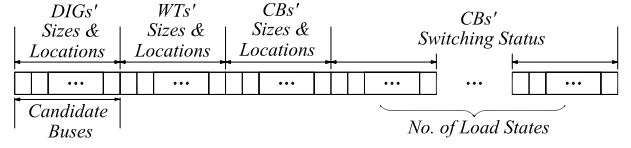
zero value in each type's vector means not to install that type at the corresponding candidate bus. The fourth vector describes the switching status of capacitor banks and is made of several sub-vectors. Each sub-vector has the same length as the first three vectors and the number of sub-vectors is equal to the number of stochastic-model's load states. These sub-vectors eventually determine that a capacitor bank is fixed or switched as follows. A capacitor bank with values of one at all load states is a fixed capacitor bank, and otherwise, the capacitor bank is a switched one. The generated chromosomes are subsequently passed to the sum-problem.

B. Optimization Sub-Problem

The power flow constraints (7)–(18) are treated as an optimization sub-problem that minimizes the l^2-norm of power-flow-mismatch equations. To this aim, a nonlinear least-squares minimization are written as

$$\min_{\mathcal{X}^{PF}} \left\| \mathbf{F}(\mathcal{X}^{PF}) \right\|_2 \tag{43}$$

where $\mathbf{F}$ represents power mismatch equations for all buses that are extracted from (7) and (8); $\mathcal{X}^{\mathbf{PF}}$ is a vector comprising magnitudes and angles of bus-voltages as well as the network frequency. This optimization sub-problem is solved using a Newton-Trust region method [19]. The power flow solution is sent back to the main problem.

VII. CASE STUDIES AND DISCUSSION

Several case studies are carried out in this section using the PG&E 69-bus system [Fig. 7] to demonstrate the effectiveness of the proposed planning platform. The system line and load-demand data can be found in [36]. A planning horizon of 20 years is assumed. The annual interest, discount, and escalation rates are considered to be 7%, 5%, and 2%, respectively. The DGs' and CBs' different costs are those used in [10]. The lines' failure rate and repair time are taken as 0.12 f/km and 8 hr, respectively, and the reliability index limit, i.e., $LOLE^U$ is equal to 450 $hr/year$. The harmonic spectrum of nonlinear loads [Fig. 7] adheres to the limits of IEEE Std. 519 [25]. The parameters of DFIG-based wind turbine applied for the harmonic analysis are also given in Table III.

TABLE III
DFIG DATA (ALL IN P.U.)

L_g	0.1980	L_f	0.1980
C_f	0.0197	L_s	0.0923
L_m	3.9528	L'_{lr}	0.0996
r_s	0.0049	r'_r	0.0055
K_p	0.3361	K_i	8.4016
ω_r	1.2	F	0

The first study reveals the significance of applying a power flow algorithm that takes into account the features of isolated microgrids, and the additional constraint introduced in Section II.B. Two scenarios are studied, each based on three 5MVA diesel generators installed at a set of three buses. Scenario 1 considers buses 1, 13, and 22. Fig. 8 shows the voltage profile at the system peak load using the power flow algorithm suitable for isolated microgrids. The reactive powers delivered by the three generators are 3.202, 0.502, and -0.925 MVAr, respectively. The significant reactive power demanded by the generator of bus 22 is because the voltage of this bus has become
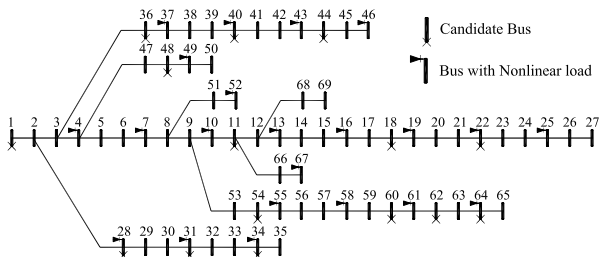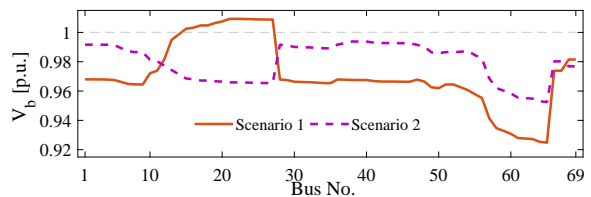
Fig. 7. The test system (PG&E 69-bus).

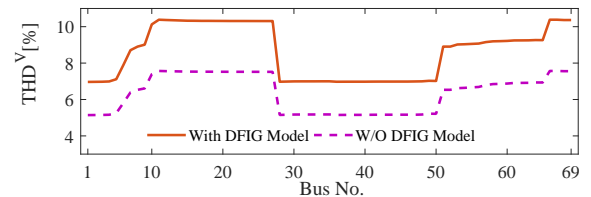Fig. 8. Impact of applying the power flow algorithm suitable for isolated microgrids and the introduced constraint.

Fig. 9. Impact of DFIG modelling in the harmonic analysis.

TABLE IV
OPTIMIZATION OUTPUTS WITHOUT VOLTAGE DISTORTION CONSTRAINT

Diesel	1.3 MVA @ Bus 28, 0.6 MVA @ Bus 44, 1.2 MVA @ Bus 54, 1.1 MVA @ Bus 64
Wind	0.3 MVA @ Bus 22, 0.5 MVA @ Bus 36
Capacitor	0.3 MVAr @ Bus 18: Fixed, 0.5 MVAr @ Bus 34: Switched, 0.5 MVAr @ Bus 48: Switched

TABLE V
OPTIMIZATION OUTPUTS WITH VOLTAGE DISTORTION CONSTRAINT

Diesel	1.4 MVA @ Bus 28, 0.4 MVA @ Bus 44, 1.5 MVA @ Bus 54, 1 MVA @ Bus 64
Wind	0.3 MVA @ Bus 22, 0.5 MVA @ Bus 36
Capacitor	0.3 MVAr @ Bus 18: Fixed, 0.4 MVAr @ Bus 34: Switched, 0.4 MVAr @ Bus 48: Switched

more than 1 p.u. [Fig. 8] while V^{nom} in (16) was 1 p.u. Several important points that can be seen are as follows. 1) The above-mentioned reactive power demand must be supplied by the two other generators, and accordingly, the system generation capacity must be increased. 2) The over-voltage is the direct consequence of applying the droop characteristics, and would not be observed if a conventional power flow were employed. The conventional power flow treats the DG buses as a PV one in which the bus voltage is assumed constant; however, it is not realistic in microgrids operated based on the droop characteristics, and a bus connected to a dispatchable DG sees a variable voltage that is determined by the load level and the slope of the droop characteristic. 3) As long as the DGs are operated based on the droop characteristics, such consequences can exist, which must be considered in the planning stage. 4) One should note that above issue was happened without the presence of any capacitors, which their presence increases the chance of facing with the issue. As for the second scenario, the diesel generators are installed at the buses 1, 38, and 54. The corresponding voltage profile at the system peak load has been shown in the same figure. The reactive powers delivered by the generators are 0.836, 0.619, and 1.270 MVAr, respectively. As can be seen, the above-mentioned issue has not been occurred. Moreover, an appropriate distribution of the DGs can lead to a significant reduction in the reactive power demand, and consequently, in the system generation capacity.

The second study is conducted to show the importance of using the proposed model for renewable DGs in the harmonic analysis. For this study, the test network is supplied by a 5 MVA diesel generator installed at Bus 1 and a 0.5 MVA DFIG-based wind turbine at Bus 11. A 0.4 MVAr shunt capacitor bank is also connected to Bus 11. Fig. 9 compares the network voltage THDs for the DFIG's simplified model of [14] and the one introduced in Section IV. As illustrated, a significant error as high of 2.8% can be expected. This voltage-THD discrepancy is attributed to the inductive/capacitive behaviour of the DFIG's harmonic impedances, and its mutual interaction with the shunt capacitor bank that leads to a quasi-resonance.

The third case study evaluates the significance of including the voltage distortion constraint in the planning. To that aim, the optimization is executed with and without the constraint. In this study, wind and load intermittencies are taken into account using Tables I and II, respectively. The candidate buses are shown in Fig. 7. Initially the optimization is considered without the voltage distortion constraint. The summary of the optimization outputs are illustrated in Table IV. As can be seen, the optimization leads to six diesel generators that are distributed throughout the network to satisfy the reliability constraint along with two wind turbines and three capacitor banks. Two capacitor banks are of switched type, and according to the optimization results should be in service for the second and third load levels. Voltage profile and voltage THD at all buses are shown in Figs. 10(a) and 10(b), respectively. As observed, the voltage profile at all buses are acceptable; however, the voltage THD at many buses are far above the permissible level of 5% [25], e.g., Bus 35 sees a voltage THD of 7.9%. Inclusion of voltage distortion constraint solves this issue. Table V illustrates the corresponding optimization outputs. Compared to the case without the distortion constraint, the size of diesel generators and capacitor banks have

been changed. Figs. 11(a) and 11(b) show both voltage profile and voltage THD are now acceptable. To quantify the cost of avoiding the voltage distortion, one can look at the annualized costs for both scenarios. While the annualized cost for the case without the voltage distortion constraint is $2.609 million, this value for the case with voltage distortion constraint is $2.622 million, which means by less than 0.5% increase in the cost, a severe distortion problem can be avoided. It is worth nothing that the above severe voltage distortion is appeared because of the presence of capacitors, and one might not see such a distortion if only allocating the DGs in a network without capacitors. This is especially the case when the nonlinear loads' harmonics are consistent with the international standards, as considered here.

VIII. CONCLUSION

In this paper a planning platform has been proposed to determine the types, sizes, and locations of DGs and CBs in an isolated microgrids with nonlinear loads. In the proposed platform, the specific features of isolated microgrids, i.e. the lack of slack bus and droop-based behaviour have of some DGs, have been taken into account for both fundamental power flow and harmonic power flow. To account for the possibility of resonance or quasi-resonance that can be caused by the wind turbines, a methodology has been proposed to incorporate them into the harmonic analysis. Eventually, given that a frequency and voltage provision cannot be provided by renewable DGs, a reliability-based technique has been proposed to
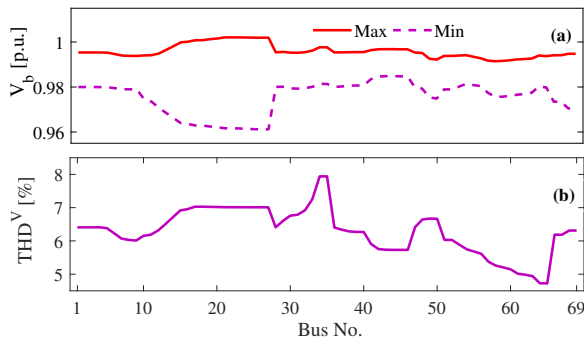
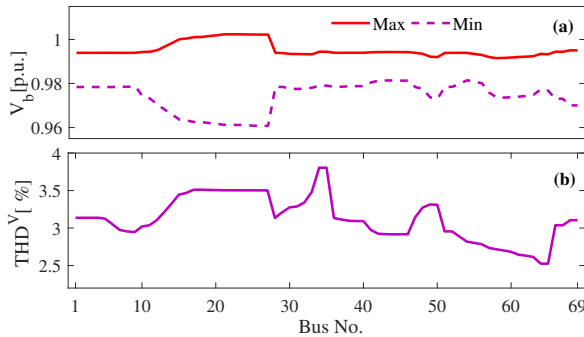Fig. 10. Planning without voltage distortion constraint.

Fig. 11. Planning with voltage distortion constraint.

distribute the dispatchable DGs throughout the microgrid, and thus, to build successful islands after a contingency.

REFERENCES

[1] IEEE Standard 1547.4, "IEEE guide for design, operation, and integration of distributed resource island systems with electric power systems," 2011.

[2] Y. A. Katsigiannis, P. S. Georgilakis, and E. S. Karapidakis, "Hybrid simulated annealing–tabu search method for optimal sizing of autonomous power systems with renewables," *IEEE Transactions on Sustainable Energy*, vol. 3, no. 3, pp. 330–338, 2012.

[3] "Microgrid Solutions for Mining. [Online]. Available:," https://new.abb.com/distributed-energy-microgrids/applications/microgrid-solutions-for-mining., accessed: 25-Dec-2018.

[4] B. Zhao, X. Zhang, P. Li, K. Wang, M. Xue, and C. Wang, "Optimal sizing, operating strategy and operational experience of a stand-alone microgrid on Dongfushan Island," *Applied Energy*, vol. 113, pp. 1656–1666, 2014.

[5] T. Ersal, C. Ahn, D. L. Peters, J. W. Whitefoot, A. R. Mechtenberg, I. A. Hiskens, H. Peng, A. G. Stefanopoulou, P. Y. Papalambros, and J. L. Stein, "Coupling between component sizing and regulation capability in microgrids," *IEEE Transactions on Smart Grid*, vol. 4, no. 3, pp. 1576–1585, 2013.

[6] H. E. Farag and E. F. El-Saadany, "Optimum shunt capacitor placement in multimicrogrid systems with consideration of islanded mode of operation," *IEEE Transactions on Sustainable Energy*, vol. 6, no. 4, pp. 1435–1446, 2015.

[7] E. Hajipour, M. Bozorg, and M. Fotuhi-Firuzabad, "Stochastic capacity expansion planning of remote microgrids with wind farms and energy storage," *IEEE transactions on sustainable energy*, vol. 6, no. 2, pp. 491–498, 2015.

[8] D. E. Olivares, A. Mehrizi-Sani, A. H. Etemadi, C. A. Cañizares, R. Iravani, M. Kazerani, A. H. Hajimiragha, O. Gomis-Bellmunt, M. Saeedifard, R. Palma-Behnke et al., "Trends in microgrid control," *IEEE Transactions on smart grid*, vol. 5, no. 4, pp. 1905–1919, 2014.

[9] A. A. Eajal and M. El-Hawary, "Optimal capacitor placement and sizing in unbalanced distribution systems with harmonics consideration using particle swarm optimization," *IEEE Transactions on Power Delivery*, vol. 25, no. 3, pp. 1734–1741, 2010.

[10] B. R. Pereira, G. R. M. da Costa, J. Contreras, and J. R. S. Mantovani, "Optimal distributed generation and reactive power allocation in electrical distribution systems," *IEEE Transactions on Sustainable Energy*, vol. 7, no. 3, pp. 975–984, 2016.

[11] J. Xiao, L. Bai, F. Li, H. Liang, and C. Wang, "Sizing of energy storage and diesel generators in an isolated microgrid using discrete Fourier transform (DFT)," *IEEE Transactions on Sustainable Energy*, vol. 5, no. 3, pp. 907–916, 2014.

[12] M. Arriaga, C. A. Caizares, and M. Kazerani, "Long-term renewable energy planning model for remote communities," *IEEE Transactions on Sustainable Energy*, vol. 7, no. 1, pp. 221–231, 2016.

[13] E. Karimi and M. Kazerani, "A Generalized Platform for Optimal Planning of Isolated Microgrids, Considering Operation Constraints," in *IECON 2018-44th Annual Conference of the IEEE Industrial Electronics Society*. IEEE, 2018, pp. 1589–1596.

[14] A. A. Abdelsalam and E. F. El-Saadany, "Probabilistic approach for optimal planning of distributed generators with controlling harmonic distortions," *IET Generation, Transmission & Distribution*, vol. 7, no. 10, pp. 1105–1115, 2013.

[15] V. R. Pandi, H. Zeineldin, and W. Xiao, "Determining optimal location and size of distributed generation resources considering harmonic and protection coordination limits," *IEEE transactions on power systems*, vol. 28, no. 2, pp. 1245–1254, 2013.

[16] Y. Song, X. Wang, and F. Blaabjerg, "High-frequency resonance damping of DFIG-based wind power system under weak network," *IEEE Transactions on Power Electronics*, vol. 32, no. 3, pp. 1927–1940, 2017.

[17] F. Wang, J. L. Duarte, M. A. Hendrix, and P. F. Ribeiro, "Modeling and analysis of grid harmonic distortion impact of aggregated DG inverters," *IEEE Transactions on Power Electronics*, vol. 26, no. 3, pp. 786–797, 2011.

[18] G. M. Masters, *Renewable and efficient electric power systems*. John Wiley & Sons, 2013.

[19] M. M. A. Abdelaziz, H. E. Farag, E. F. El-Saadany, and Y. A.-R. I. Mohamed, "A novel and generalized three-phase power flow algorithm for islanded microgrids using a newton trust region method," *IEEE Transactions on Power Systems*, vol. 28, no. 1, pp. 190–201, 2013.

[20] Y. Li, D. M. Vilathgamuwa, and P. C. Loh, "Design, analysis, and real-time testing of a controller for multibus microgrid system," *IEEE Transactions on power electronics*, vol. 19, no. 5, pp. 1195–1204, 2004.

[21] H. Mahmood, D. Michaelson, and J. Jiang, "Accurate reactive power sharing in an islanded microgrid using adaptive virtual impedances," *IEEE Transactions on Power Electronics*, vol. 30, no. 3, pp. 1605–1617, 2014.

[22] NERC Standard, "TOP-004–2: Transmission Operations," *North American Electric Reliability Corporation*, 2007.

[23] J. Rocabert, A. Luna, F. Blaabjerg, and P. Rodriguez, "Control of power converters in AC microgrids," *IEEE transactions on power electronics*, vol. 27, no. 11, pp. 4734–4749, 2012.

[24] J. He and Y. W. Li, "Hybrid voltage and current control approach for DG-grid interfacing converters with LCL filters," *IEEE Transactions on Industrial Electronics*, vol. 60, no. 5, pp. 1797–1809, 2013.

[25] "519-2014-IEEE Recommended Practice and Requirements for Harmonic Control in Electric Power Systems," *IEEE Std 519-2014*, pp. 1–29, 2014.

[26] P. CODE and C. PRIX, "Electromagnetic compatibility (EMC)–Part 3-7: Limits–Assessment of emission limits for the connection of fluctuating installations to MV, HV and EHV power systems," 2008.

[27] Task Force, "Characteristics and modeling of harmonic sources-power electronic devices," *IEEE Power Engineering Review*, vol. 21, no. 8, pp. 62–63, 2001.

[28] Y. Song, X. Wang, and F. Blaabjerg, "Impedance-based high-frequency resonance analysis of DFIG system in weak grids," *IEEE Transactions on Power Electronics*, vol. 32, no. 5, pp. 3536–3548, 2016.

[29] Z. Miao, "Impedance-model-based SSR analysis for type 3 wind generator and series-compensated network," *IEEE Transactions on Energy Conversion*, vol. 27, no. 4, pp. 984–991, 2012.

[30] N. Mohan and T. M. Undeland, *Power electronics: converters, applications, and design*. John wiley & sons, 2007.

[31] P. Krause, "Oleg; Sudhoff, Scott D; Pekarek, Steven," *Analysis of electric machinery and drive systems*, vol. 75, 2013.

[32] P. Vas, *Sensorless vector and direct torque control*. Oxford Univ. Press, 1998.

[33] Y. Song and F. Blaabjerg, "Wide frequency band active damping strategy for DFIG system high frequency resonance," *IEEE Transactions on Energy Conversion*, vol. 31, no. 4, pp. 1665–1675, 2016.

[34] M. A. Alotaibi and M. M. Salama, "An incentive-based multistage expansion planning model for smart distribution systems," *IEEE Transactions on Power Systems*, vol. 33, no. 5, pp. 5469–5485, 2018.

[35] Task Force, "The IEEE Reliability Test System," *IEEE Transactions on Power Systems*, vol. 14, no. 3, pp. 1010–1020, Aug 1999.

[36] M. E. Baran and F. F. Wu, "Optimal capacitor placement on radial distribution systems," *IEEE Transactions on power Delivery*, vol. 4, no. 1, pp. 725–734, 1989.